MATERIALS CHEMISTRY
FRONTIERS

RESEARCH ARTICLE

View Article Online
View Journal | View Issue

Cite this: *Mater. Chem. Front.*, 2018, **2**, 1317

A single palladium site catalyst as a bridge for converting homogeneous to heterogeneous in dimerization of terminal aryl acetylenes†

Chao Zhao,‡[a] Haizhu Yu,‡[d] Jing Wang,[a] Wei Che,[c] Zhijun Li,[a] Tao Yao,[c] Wensheng Yan,[c] Min Chen,[a] Jian Yang,[a] Shiqiang Wei,[c] Yuen Wu*[a] and Yadong Li[b]

Received 7th March 2018,
Accepted 25th March 2018

DOI: 10.1039/c8qm00095f

rsc.li/frontiers-materials

Herein, we utilize the surface dangling bond of MOFs as anchoring sites to access single Pd sites embedded on a hollow MOF nanobox. The stabilization of isolated Pd_1 species is based on the strong coordination of the surface dangling bond of MOFs, followed by sequential reduction and phase transfer processes. The supported isolated single Pd sites can effect the highly active and selective process to produce conjugated dienes towards the dimerization of terminal aryl acetylenes, which has been previously only catalyzed by homogeneous catalysts. Unlike the commercial Pd/C and nanoparticles (NPs), the heterolytic cleavage of H_2 and C–H bond efficient cleavage of terminal alkynes on atomically dispersed Pd_1 sites ensure the high selectivity process and prevent the generation of styrene.

Introduction

Heterogeneous catalysts with satisfactory recyclability and easy separation have been widely used in the modern chemical industry. In the past decades, metal NP catalysts have achieved overwhelming successes in organocatalysis and electrocatalysis by realizing the activation of small molecules such as hydrogen, oxygen and carbon dioxides.[1–12] Unlike the homogeneous catalysts commonly adopting well-defined metal centers and ligands, the diverse distribution of reactive sites and the coexistence of multiple surface configurations usually cause the reactions catalyzed by NP catalysts to occur *via* multifarious pathways. To date, the catalytic reactions realized by NP catalysts are mostly limited to oxidation/reduction and cross-coupling reactions.[1] Towards the synthesis of complex molecules and chemicals involving more restructuring of the chemical bonds and intricate mechanisms, the homogeneous catalysts still remain the most powerful tools for the synthetic chemists. Still, it is highly desirable to exploit new catalytic systems that combine the versatility and selectivity of homogeneous catalysts and the fascinating features of heterogeneous catalysis.[13–15]

Single site catalysts (SSCs) with well-defined single metal centers on a defect-rich support surface based on the strong Lewis acid–base interplay have become one of the new frontiers and hot spots in heterogeneous catalysis.[16–21] Apart from the advantages attributed to heterogeneous catalysts including stability and reusability, the single site catalysts can serve as a promising alternative to heterogenize the homogeneous catalysts due to their unique quantum size effect, low-coordination environment and metal–support interactions.[22,23] Towards the important transformations in homogeneous catalysis and biocatalysis, the unique interplay between the ligands and metal centres often guarantees the excellent selectivity of the

[a] *Department of Chemistry, iChEM (Collaborative Innovation Center of Chemistry for Energy Materials), University of Science and Technology of China, Hefei 230026, China. E-mail: yuenwu@ustc.edu.cn*
[b] *Department of Chemistry, Tsinghua University, Beijing 100084, China*
[c] *National Synchrotron Radiation Laboratory, University of Science and Technology of China, Hefei 230029, China*
[d] *Department of Chemistry and Center for Atomic Engineering of Advanced Materials, Anhui Province Key Laboratory of Chemistry for Inorganic/Organic Hybrid Functionalized Materials, Anhui University, Hefei, 230601, China*
† Electronic supplementary information (ESI) available. See DOI: 10.1039/c8qm00095f
‡ These authors contributed equally.

Yuen Wu

Yuen Wu received his BS and PhD degrees from the Department of Chemistry, Tsinghua University in 2009 and 2014, respectively. He is currently a professor in the Department of Chemistry, University of Science and Technology of China. His research interests are focused on the synthesis, assembly, characterization and application exploration of functional nanomaterials.

homogeneous catalysts due to the well-defined geometric and electronic structures.[24–26] Recently, the single site catalysts have been confirmed to be very selective for some important reactions including hydroformylation of olefins,[23] electroreduction of carbon dioxide,[27] electroreduction of oxygen to hydrogen peroxide,[28] and so on.[29] To some extent, the defects on the support such as oxygen vacancies or carbon vacancies can serve as organic modifiers (ligands) to make the SSCs behave like their homogeneous analogues and offer high selectivity towards a specific product.[18,30] Therefore, it is highly believed that SSCs could bridge the gap between homogeneous and heterogeneous catalysis.[18,23]

To date, conjugated dienes are mainly produced by the Suzuki–Miyaura cross-coupling reaction, which has been exclusively achieved with expensive and environmentally unfriendly homogeneous catalysts (for example, copper salts, and palladium complexes).[31–36] It remains a bottleneck to effectively generate conjugated dienes using recoverable and environmentally benign heterogeneous catalysts. Herein, we demonstrate that single Pd site catalysts can achieve a heterogenized process of homogeneous catalysts in the dimerization of terminal aryl acetylenes. Such an isolated Pd_1 species exhibits high selectivity towards producing conjugated dienes, a very important class of intermediates in the synthesis of pharmaceuticals, pesticides, rubber and other chemical products.[28,31] Density functional theory (DFT) calculations reveal that the heterolytic cleavage of H_2 and the C–H bond efficient activation of terminal alkynes on Pd_1 sites ensure the highly selectivity process.

In this work, we utilize the surface coordinatively unsaturated dangling N bond of ZIF-67 to synthesize a novel isolated single Pd site on a hollow MOF nanobox catalyst (denoted as Pd_1/H-ZIF). The synthesis is based on the strong coordination between the lone pair electrons from the free amine groups and Pd d-orbital, enabling the atomic dispersion of surface Pd sites (Fig. 1a). During the catalytic reaction, the reactants could easily interact with the active sites without the limitation of mass diffusion due to the accessible surface.

Results

Synthesis and structure characterization of Pd_1/H-ZIF

Zeolite imidazolate frameworks (ZIF-67) with uniform rhombic dodecahedron and excellent monodispersity were synthesized *via* a hydrothermal method, as evidenced by transmission electron microscopy (TEM) (Fig. 1b and Fig. S1, ESI†). As illustrated in Fig. 1a, the as-prepared ZIF-67, comprising similar sodalite coordination of Co^{2+} nodes and 2-methylimidazole, was used as a support to anchor Pd species with the surface unsaturated dangling N groups. Firstly, Na_2PdCl_4 was introduced into a turbid liquid of ZIF-67 to allow the full absorption of Pd due to the strong coordination interaction between Pd^{2+} and N. After being collected and washed with methanol, the resulting $PdCl_2$/ZIF-67 was annealled at 200 °C under an H_2/Ar atmosphere to reduce the isolated ionic Pd atoms and remove the coordinative Cl^-. The as-obtained powders were re-dispersed

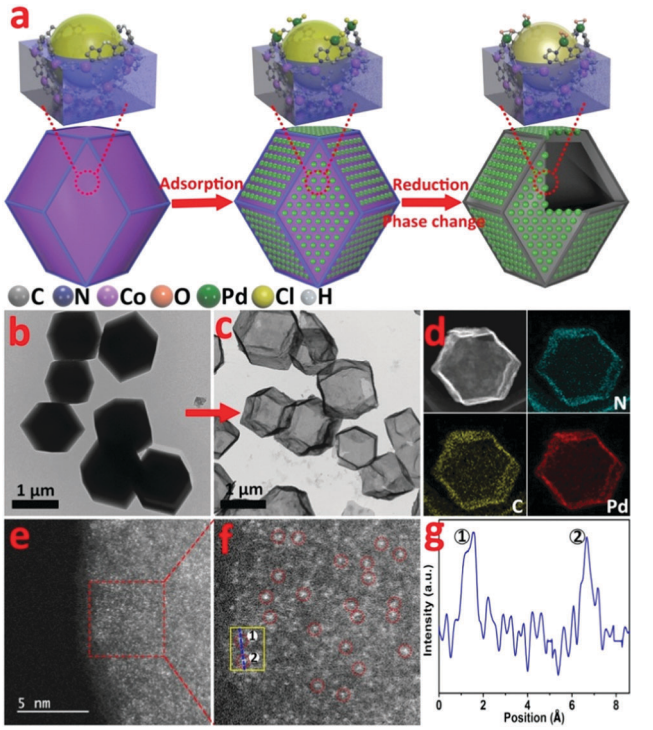

Fig. 1 (a) Schematic illustration of the preparation of Pd_1/H-ZIF, (b) TEM image of ZIF-67, (c) TEM image of Pd_1/H-ZIF, (d) corresponding EDS mapping images of N, C and Pd, (e and f) magnified HAADF-STEM images of Pd_1/H-ZIF, showing that only Pd atoms are present in Pd_1/H-ZIF, and (g) the corresponding intensity profiles obtained on the yellow area in (f).

in deionized water and heated at 100 °C for 2 h, during which a mild phase transformation occurred under hydrothermal conditions. As verified by the evolution from Fig. 1b to c, the internal ZIF-67 core was gradually dissolved after the phase change process, leaving a stable hollow residue (Pd_1/H-ZIF). The obtained Pd_1/H-ZIF catalyst has a uniform hollow rhombic dodecahedron shell structure, without the formation of Pd NPs. Energy dispersive X-ray spectroscopy (EDS) analysis in a scanning transmission electron microscope (STEM) identified that the Pd atoms were successfully anchored within the remaining shell (Fig. 1d). This result indicated that the Pd–N coordination is more stable than Co–N coordination in the presence of water (Fig. 2a). To further elucidate the existence form of the as-grown Pd atoms, aberration corrected high-angle annular dark-field scanning transmission electron microscopy (HAADF-STEM) (Fig. 1e and Fig. S3, ESI†) was conducted. As a result, the isolated Pd atoms with brighter contrast could be discerned (Fig. 1f), underlying the atomic dispersion and reinforcing the stability of Pd–N coordination. The loading of Pd was 1.81%, which was measured by inductively coupled plasma atomic emission spectrometry (ICP-AES). The intensity profiles obtained from the yellow area in Fig. 1f clearly illustrate that the intensity of the two bright dots is obviously different from the neighbouring atoms due to their higher Z-contrast, further proving the isolated Pd atoms in Pd_1/H-ZIF (Fig. 1g).

The representative steps for the synthesis of Pd_1/H-ZIF and the corresponding crystalline phase evolution were firstly investigated

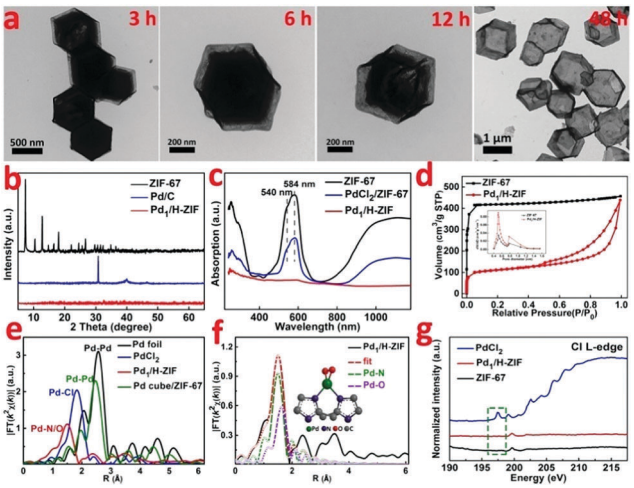

Fig. 2 (a) The phase change process of Pd_1/H-ZIF at room temperature, (b) XRD, (c) UV/Vis diffuse reflection spectrum, (d) nitrogen adsorption isotherm and desorption isotherm, (e) the k_3-weighted $\chi(k)$-function of the EXAFS spectra, (f) the corresponding Pd K-edge EXAFS fitting curves of Pd_1/H-ZIF, and (g) Cl L-edge spectra.

by X-ray diffraction (XRD). As shown in Fig. 2b, the adsorption of Pd^{2+} would not induce structural damage of the ZIF-67, because most of the Pd^{2+} only coordinated with the surface N atoms from the ligands. However, after the hydrothermal treatment, the characteristic peaks of ZIF-67 completely disappeared when compared to the as-prepared Pd_1/H-ZIF, evidencing the dissolution of the ZIF-67 core. Moreover, there were no observable characteristic crystal peaks of Pd NPs in the XRD patterns of Pd_1/H-ZIF as compared to Pd/C, further excluding the formation of large particles (Fig. 2b and Fig. S7, ESI†). The phase change coincided well with the results obtained by UV/Vis diffuse reflection spectroscopy (Fig. 2c). That is, the peaks at 584 nm and 540 nm are characteristic of Co^{2+} in tetrahedral coordination with N in ZIF-67. The evanishment of these peaks suggested the degradation of the Co–N coordination mode along with the phase transformation. It was proposed that water molecules may be involved in the unit cell by forming H-bonds. This interaction may affect the coordination mode between Co^{2+} and 2-methylimidazole, which drives the structural evolution from ZIF-67 to a hollow rhombic dodecahedron shell structure. Surprisingly, the surface Pd–N coordination is much stronger than Co–N coordination, guaranteeing the robustness of the hollow rhombic dodecahedron shell structure under hydrothermal conditions. ICP indicated that the residual content of Co was 5.63%, which was used to maintain the hollow shell structure. A color variation from purple to gray was also observed for samples collected during the evolution process from ZIF-67 to Pd_1/H-ZIF (Fig. S8, ESI†). Thermogravimetric analysis (TGA) demonstrated that the stability of the Pd_1/H-ZIF improves obviously after the phase transformation (Fig. S9, ESI†). Brunauer–Emmett–Teller (BET) adsorption–desorption isotherms indicated that the surface area of the hollow Pd_1/H-ZIF was 355.4 $m^2\ g^{-1}$ (Fig. 2d).

The X-ray absorption near edge structures (XANES) of the Pd K-edge for the Pd_1/H-ZIF catalyst and reference materials of Pd foil, a Pd cube and PdO are shown in Fig. S10 and S11 (ESI†). In comparison with the Pd foil and Pd cube, the white line of Pd_1/H-ZIF shows a small shift to higher energy for the absorption edge (E_0), and the near-edge structure was similar to PdO, suggesting that the valence state of $Pd^{\delta+}$ in Pd_1/H-ZIF is more positive than Pd^0 and negative than Pd^{2+}. This conclusion was corroborated by the X-ray photoelectron spectroscopy (XPS) measurements, which also revealed that the valence states of Pd were positively charged between 0 and +2 (Fig. S12, ESI†). To further analyze the atomic structure of Pd_1/H-ZIF, we performed extend X-ray absorption fine structure (EXAFS) spectroscopy at the Pd K-edge to probe the detailed electronic structure and coordination environment (Fig. 2e). Different from the Pd foil and Pd cube, both of which have obvious peaks in the region of 2 to 3 Å assigned to the Pd–Pd contribution, there was only one notable peak in the region of 1 to 2 Å for Pd_1/H-ZIF. In contrast to the Pd–Cl bond contribution in $PdCl_2$, the peak of Pd_1/H-ZIF with a smaller R value should result from the mixture of the Pd–N and Pd–O contributions (Fig. 2f). Meanwhile, according to the fitting results presented in Table S1 and Fig. S13 (ESI†), the coordination numbers of Pd–N and Pd–O were 2 and 2, respectively. The surface N atoms of the support bridge the Pd atoms with a Pd–N bond and the oxygen coordinates with a Pd–O bond, as shown in the calculated structure model in Fig. 2e. In addition, the Cl L-edge X-ray absorption spectroscopy (XAS) spectra confirmed that no Pd–Cl bond signal was found for Pd_1/H-ZIF (Fig. 2g), in line with the EXAFS spectra.

Catalytic measurements of Pd_1/H-ZIF

Table S2 (ESI†) shows the catalytic performances of a wide range of Pd-based homogeneous and heterogeneous catalysts including salts, complexes, and different Pd supported species for the dimerization of phenylacetylene to generate conjugated dienes. The result is that only Pd_1/H-ZIF exhibited high selectivity to access conjugated dienes in high yield (entry 1). As indicated by GC-MS and ^{1}H NMR spectroscopy, 1,4-diphenyl-1,3-butadiene ((*E*,*E*) isomer) was observed as a major product, along with by products such as styrene and cyclotrimerization products. Meanwhile, GC-MS revealed that two additional species, with the same mass and similar GC retention time to the (*E*,*E*) isomer (presumably the (*E*,*Z*) and (*Z*,*Z*) isomers), were present in all reaction samples in a low concentration (13% of the (*E*,*E*) isomer concentration).

For tests on different Pd salts and complexes (entries 9–14), we notice that such a reaction process was catalyzed by Pd^{2+} rather than Pd^0, which is in good agreement with the existence of $Pd^{\delta+}$ for Pd_1/H-ZIF. By contrast, the ZIF-67 did not show any observable catalytic activity, implying the crucial role of $Pd^{\delta+}$ centers instead of the MOF substrate (entry 8). It is reasonable that the hydrogenation reaction catalyzed by the heterogeneous Pd NPs mainly delivers the full hydrogenation products of styrene (entries 2–4). This poor selectivity to conjugated dienes was attributed to the complex reactive sites on Pd NPs and the easy cleavage of a H–H bond on a Pd surface. The Pd cube@ZIF-67 exhibited negligible catalytic activity as compared with Pd cube/ZIF-67,

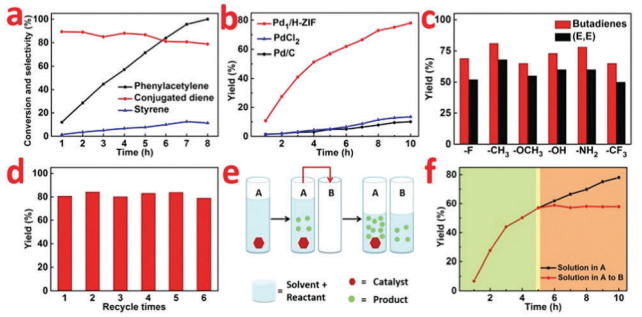

Fig. 3 (a) Time-dependent catalysis by the Pd_1/H-ZIF. (b) Reaction performances for Pd_1/H-ZIF, Pd/C and $PdCl_2$ in dimerization of phenylacetylene to generate a conjugated diene. (c) Catalytic performances for dimerization of substituted phenylacetylene over the Pd_1/H-ZIF. (d) The recyclability of Pd_1/H-ZIF. (e and f) Hot filtration test.

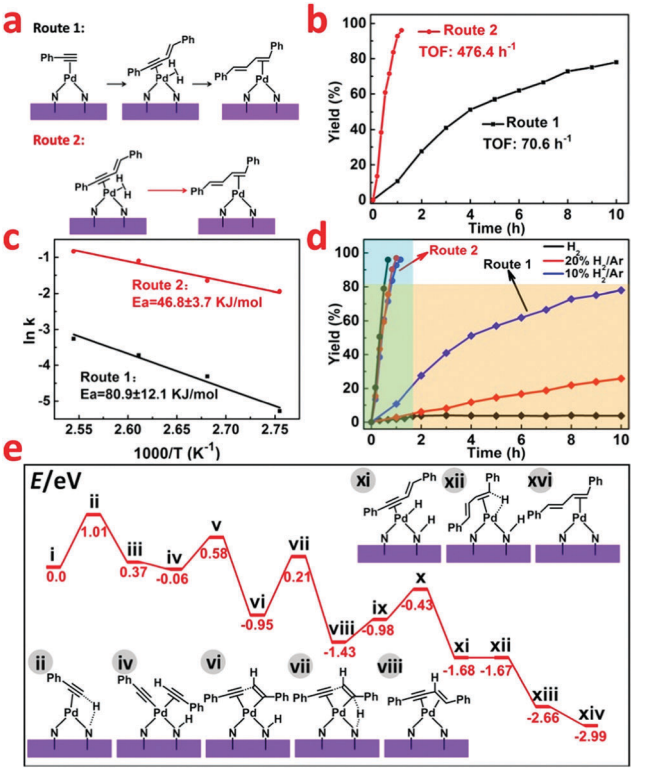

Fig. 4 (a and b) Different routes in the reaction process. (c) Arrhenius plot of the different reaction routes for Pd_1/H-ZIF. (d) The influence of different atmospheres in different routes. (e) Energies of intermediates and transition states in the mechanism of phenylacetylene dimerization at the Pd_1/H-ZIF from DFT calculations.

which demonstrated that the catalysis process occurs on the surface of the catalyst (entry 5).

The variation of conversion and selectivity as a function of reaction time were further determined to track the reaction kinetics (Fig. 3a and b). In contrast to Pd_1/H-ZIF, the $PdCl_2$ and commercial Pd/C both exhibited poor selectivity toward conjugated dienes, leading to the formation of styrene and ethylbenzene as the main products. When phenylacetylene was fully converted, the yields of conjugated diene were only 13.1% and 9.8%, respectively (Fig. 3b). To strengthen the general applicability, we further adopted a series of terminal aryl acetylenes with different substitutions (Fig. 3c), including 1-fluoro-4-phenylacetylene, 1-methyl-4-phenylacetylene, 1-methoxy-4-phenylacetylene, 1-hydroxy-4-phenylacetylene, 1-amino-4-phenylacetylene, and 1-trifluoromethyl-4-phenylacetylene, as the substrates under the catalysis of Pd_1/H-ZIF. As a new promising heterogeneous catalyst, the Pd_1/H-ZIF also exhibited excellent stability and recyclability, as verified by invariant activity and selectivity for more than six cycles of catalysis (Fig. 3d).

To further confirm that the catalysis over Pd_1/H-ZIF underwent a heterogeneous process and the active Pd_1 species were not leaching to form a homogeneous active catalyst, a hot Filtration test was performed. A mixture of the substrate, Pd_1/H-ZIF, and solvent were added to a vessel (A) to generate products (Fig. 3e and f). When the reaction in vessel (A) reached 57% yield, half of the solution after the removal of the catalysts was placed into a new vessel (B) without catalyst. The catalyst of Pd_1/H-ZIF was preserved in (A). Both vessels A and B were then stirred and monitored under the same reaction conditions. The yield in B remained constant (red section), whereas the reaction in (A) continued to generate the product (black section). This further indicated that the active species was a heterogeneous catalyst rather than leached homogeneous Pd species. Elemental analysis by ICP of B also showed that there was no observable soluble Pd species detected above the instrument's detection limits. Together, this collection of experiments strongly supports that the catalytically active species is the heterogeneous Pd_1/H-ZIF, rather than homogeneous species that were leached from the Pd_1/H-ZIF during the reaction.

In the catalytic reaction process, slight 1,3-enyne intermediate was caught by GC-MS, which suggests that the activation of a terminal C–H bond in phenylacetylene might be a crucial step for the C–C coupling (Fig. 4a). To verify this hypothesis and further explore the reaction mechanism, we used 1,3-enyne as the reactant under the same hydrogenation conditions. As shown in Fig. 4b, 1,3-enyne was rapidly catalyzed to generate a conjugated diene with a higher TOF value of 476.4 h^{-1} (Route 2), whereas the starting material of phenylacetylene only delivered a TOF of 70.6 h^{-1} (Route 1). For these two different reaction routes, the corresponding activation energy (E_a) calculated based on the Arrhenius plot were 80.9 ± 12.1 KJ mol^{-1} (Route 1) and 46.8 ± 3.7 KJ mol^{-1} (Route 2), respectively (Fig. 4c). This indicated that the generation of 1,3-enyne is much slower than the following hydrogenation process to conjugated diene. Based on the above findings, we find the sequential C–C coupling of phenylacetylene and hydrogenation of 1,3-enyne. The selectivity of the hydrogenation of phenylacetylene catalyzed by Pd_1/H-ZIF (Route 1) was highly sensitive to the concentration of hydrogen (Fig. 4d). That is, the dimerization of phenylacetylene was mainly accessed under the 10% H_2/Ar conditions with up to 80.7% yield and the yield to styrene was restrained to 8.0%. If the hydrogenation atmosphere was changed to 20% H_2/Ar or pure H_2, the yield to styrene would significantly increase to 12.5% and 90.3%, respectively (Table S3, ESI†). Under a H_2-free environment, the cyclotrimerization of phenylacetylene would dominantly occur with a quite

sluggish rate (19.87% yield in 10 h). In contrast, the selectivity of hydrogenation of 1,3-enyne (Route 2) almost remained unchanged under different H_2 concentrations (Fig. 4d). These results implied that the competition between the coupling of two phenylacetylenes and the hydrogenation of C≡C was crucial for the selectivities towards conjugated diene and styrene, which was strictly regulated by the isolated Pd_1 sites and hydrogen concentration.

Discussion

According to our DFT calculations, the N group on the support could act as a flexible H-transfer agent throughout the reaction process. More importantly, the activation of H_2 in a heterolytic pathway over the isolated atomic Pd_1 sites on Pd_1/H-ZIF ensured the high selectivity to conjugated diene and styrene generation. As shown in Fig. 4e and Fig. S16 (ESI†), at first, the C–H bond efficient activation of terminal alkynes occurred on Pd_1 sites. And the coupling is initiated by the H-transfer from the alkyne to the N group *via* the transition state ii. The energy barrier for this step is calculated to be 1.01 eV. After that, the formed intermediate iii easily undergoes the coordination of another alkyne substrate to form the intermediate iv. The C–C bond formation and the H-transfer (from the N group to the alkene group) occur on single Pd_1 sites successively to generate the 1,3-enyne coordinated intermediate viii. Throughout the transformation from i to viii, the second H-transfer is the rate-determining step, and the overall activation energy barrier is determined to be 1.16 eV (vi → vii → viii). From viii, the following hydrogenation of the alkyne group was also facilitated by cleavage of H_2 over a Pd–N site. As shown in Fig. S16 (ESI†), after the coordination of one H_2 molecule, the H-transfer to the N group occurs prior to the hydrogenation step (ix → x → xi → xii → xiii). Finally, a subsequent H-transfer (from the N group) to the internal C atom of the enyne substrate (xiii → xiv) occurs to generate the formation of the coupling product. From Fig. 4e, the overall activation energy barrier for the transformation from xi to xiv is 1.0 eV. The relatively low energy barrier in the hydrogenation step of 1,3-enyne (compared to that in the 1,3-enyne formation step, 1.16 eV) indicates that the step of C–C bond formation dominates the overall reaction rates. This conclusion correlates well with the experimental observations.

Conclusions

In summary, we successfully synthesized Pd_1/H-ZIF by utilizing the surface unsaturated dangling bond of MOFs. Such a single site catalyst achieves a heterogeneous catalytic process with high selectivity in dimerization of terminal aryl acetylenes, which has been previously only catalyzed by homogeneous catalysts. This work can provide a framework for rationally designing highly efficient heterogeneous catalysts, and further insight into the relationship of the catalytic mechanism and structure of catalysts at the atomic scale.

Author contributions

Y. E. W. and Y. D. L. conceived the idea and co-wrote the paper. C. Z. carried out the sample synthesis, characterization and measurement. J. W, Z. J. L, M. C and J. Y helped with the characterization and measurement. T. Y., W. C., W. S. Y. and S. Q. W. helped with the XAFS measurements and discussion. H. Z. Y. performed DFT calculations. All the authors contributed to the overall scientific interpretation and edited the manuscript.

Conflicts of interest

There are no conflicts to declare.

Acknowledgements

This work was supported by the National Key R&D Program of China 2017YFA (0208300), and the National Natural Science Foundation of China (21522107, 21671180, 21521091, 21390393, and U1463202). This work made use of the resources and finance support of the National Synchrotron Radiation Laboratory in Beijing and Shanghai. We thank the Photoemission End stations (BL10B) in the National Synchrotron Radiation Laboratory (NSRL) for help in characterization.

Notes and references

1 H. Cong and J. A. Porco Jr, *ACS Catal.*, 2012, **2**, 65.
2 M. Boronat and A. Corma, *Acc. Chem. Res.*, 2014, **47**, 834.
3 Q. Fu, H. Saltsburg and M. Flytzani-Stephanopoulos, *Science*, 2003, **301**, 935.
4 X. Guo, G. Fang, G. Li, H. Mao, H. Fan, X. Pan and X. Bao, *Science*, 2014, **344**, 616.
5 K. Ding, A. Gulec, A. M. Johnson, N. M. Schweitzer, G. D. Stucky, L. D. Marks and P. C. Stair, *Science*, 2015, **350**, 189.
6 J. H. Kwak, J. Mei, D. Hu, C. W. Yi, D. H. Kim, C. H. F. Peden, L. F. Allard and J. Szanyi, *Science*, 2009, **325**, 1670.
7 Y. Zhai, D. Pierre, R. Si, W. Deng, P. Ferrin, M. Mavrikakis and M. Flytzani-Stephanopoulos, *Nat. Chem.*, 2010, **2**, 36.
8 J. Zhang, B. An, Y. Hong, Y. Meng, X. Hu, C. Wang, J. Lin, W. Lin and Y. Wang, *Mater. Chem. Front.*, 2017, **1**, 2405.
9 Y. Lei, Y. Wan, G. Li, X. Zhou, Y. Gu, J. Feng and R. Wang, *Mater. Chem. Front.*, 2017, **1**, 1541.
10 L. Oar-Arteta, T. Wezendonk, X. Sun, F. Kapteijn and G. Gascon, *Mater. Chem. Front.*, 2017, **1**, 1709.
11 A. Balram, H. Zhang and S. Santhanagopalan, *Mater. Chem. Front.*, 2017, **1**, 2376.
12 M. Asnavandi and C. Zhao, *Mater. Chem. Front.*, 2017, **1**, 2541.
13 C. A. Witham, W. Huang, C. K. Tsung, J. N. Kuhn, G. A. Somorjai and F. D. Toste, *Science*, 2009, **323**, 760.
14 W. Huang, J. H. Liu, P. Alayoglu, Y. Li, F. D. Toste and G. A. Somorjai, *J. Am. Chem. Soc.*, 2010, **132**, 16771.
15 R. Ye, A. V. Zhukhovitskiy, C. V. Deraedt, F. D. Toste and G. A. Somorjai, *Acc. Chem. Res.*, 2017, **50**, 1894.
16 B. Qiao, A. Wang, X. Yang, L. F. Allard, Z. Jiang, Y. Cui, J. Liu, J. Li and T. Zhang, *Nat. Chem.*, 2011, **3**, 634.

17 Z. Wang, L. Gu, L. Song, H. Wang and R. Yu, *Mater. Chem. Front.*, 2018, DOI: 10.1039/c8qm00081f.
18 P. Liu, Y. Zhao, R. Qin, S. Mo, G. Chen, G. Fu and N. F. Zheng, *Science*, 2016, **352**, 797.
19 P. Yin, T. Yao, Y. Wu, L. Zheng, Y. Lin, W. Liu, H. Ju, J. Zhu, X. Hong, Z. Deng, G. Zhou, S. Wei and Y. Li, *Angew. Chem., Int. Ed.*, 2016, **55**, 10800.
20 X. Wang, W. Chen, L. Zhang, T. Yao, W. Liu, Y. Lin, Y. Wu and Y. Li, *J. Am. Chem. Soc.*, 2017, **139**, 9419.
21 H. Yan, H. Cheng, H. Yi, Y. Lin, T. Yao, C. Wang and J. L. Lu, *J. Am. Chem. Soc.*, 2015, **137**, 10484.
22 X. F. Yang, A. Wang, B. Qiao, J. Li, J. Liu and T. Zhang, *Acc. Chem. Res.*, 2013, **46**, 1740.
23 R. Lang, T. Li, D. Matsumura, S. Miao, Y. Ren, Y. Cui and T. Zhang, *Angew. Chem., Int. Ed.*, 2016, **55**, 16054.
24 A. Schmid, *Nature*, 2001, **409**, 258.
25 D. H. Wang, K. M. Engle, B.-F. Shi and J. Q. Yu, *Science*, 2010, **327**, 315.
26 G. F. Swiegers, *Mechanical Catalysis: Methods of Enzymatic, Homogeneous, and Heterogeneous Catalysis*, JohnWiley, 2008.
27 C. Zhao, X. Dai, T. Yao, W. Chen, X. Wang, J. Wang, Y. Wu and Y. Li, *J. Am. Chem. Soc.*, 2017, **139**, 8078.
28 S. Yang, J. Kim, Y. J. Tak, A. Soon and H. Lee, *Angew. Chem., Int. Ed.*, 2016, **55**, 2058.
29 E. J. Peterson, A. T. DeLaRiva, S. Lin, R. S. Johnson, H. Guo and J. T. Miller, *Nat. Commun.*, 2014, **5**, 4885.
30 G. Chen, C. Xu, X. Huang, J. Ye, L. Gu, G. Li, G. Fu and N. F. Zheng, *Nat. Mater.*, 2016, **15**, 564.
31 S. A. Rao and M. Periasamy, *J. Chem. Soc., Chem. Commun.*, 1987, 495.
32 Y. Yamamoto, H. Yatagai, K. Maruyama, A. Sonoda and S. I. Murahashi, *J. Am. Chem. Soc.*, 1977, **99**, 5652.
33 M. Wilklow-Marnell, B. Li, T. Zhou, K. Krogh-Jespersen, W. W. Brennessel and T. J. Emge, *J. Am. Chem. Soc.*, 2017, **139**, 8977.
34 R. C. Larock, *J. Org. Chem.*, 1976, **41**, 2241.
35 N. Satyanarayana and M. Periasamy, *Tetrahedron Lett.*, 1986, **27**, 6253.
36 S. Ren, T. Seki, D. Necas, H. Shimizu, K. Nakajima and K.-i. Kanno, *Chem. Lett.*, 2011, **40**, 1443.

